



HAL
open science

An accuracy comparison of piecewise linear reconstruction techniques for the characteristic finite volume method for two-dimensional convection-diffusion equations

Kanokwarun Para, Bubpha Jitsom, Robert Eymard, Surattana Sungnul,
Sekson Sirisubtawee, Sutthisak Phongthanapanich

► To cite this version:

Kanokwarun Para, Bubpha Jitsom, Robert Eymard, Surattana Sungnul, Sekson Sirisubtawee, et al.. An accuracy comparison of piecewise linear reconstruction techniques for the characteristic finite volume method for two-dimensional convection-diffusion equations. *Journal of Applied Mathematics and Mechanics / Zeitschrift für Angewandte Mathematik und Mechanik*, 2021, 101 (12), 10.1002/zamm.201900245 . hal-03319127

HAL Id: hal-03319127

<https://hal.science/hal-03319127>

Submitted on 11 Aug 2021

HAL is a multi-disciplinary open access archive for the deposit and dissemination of scientific research documents, whether they are published or not. The documents may come from teaching and research institutions in France or abroad, or from public or private research centers.

L'archive ouverte pluridisciplinaire **HAL**, est destinée au dépôt et à la diffusion de documents scientifiques de niveau recherche, publiés ou non, émanant des établissements d'enseignement et de recherche français ou étrangers, des laboratoires publics ou privés.

An accuracy comparison of piecewise linear reconstruction techniques for the characteristic finite volume method for two-dimensional convection-diffusion equations

Kanokwarun Para*, Bubpha Jitsom*, Robert Eymard[†]
Surattana Sungnul*, Sekson Sirisubtawee* and Sutthisak Phongthanapanich[‡]

August 11, 2021

Abstract

In this paper, we apply the characteristic finite volume method (CFVM) for solving a convection-diffusion problem on two-dimensional triangular grids. The finite volume method is used to discretize the equation while the finite element method is applied to estimate the gradient quantities at cell faces. The numerical analysis of the convergence has been implemented for the CFVM in one-dimension. The approximate L_2 norm of the error is derived to determine the errors for the approximate solution. The accuracy of four piecewise linear reconstruction techniques, namely, Frink, Holmes-Connell, Green-Gauss, and least-squares methods are investigated on structured triangular grids. Numerical evidence shows that the least-squares method is the most accurate of all methods for smooth initial condition problems. For discontinuous initial condition problems, the Frink and the Holmes-Connell methods give a spurious oscillating solution in the vicinity of the discontinuity upstream of the discontinuity, and the Green-Gauss and least-squares methods give a spurious oscillating solution in the vicinity of the discontinuity downstream of the discontinuity. Moreover, the amplitude of the oscillation could be amplified on the finer grid sizes.

Keywords: characteristic finite volume method, convection-diffusion equation, piecewise linear reconstruction, two-dimensional triangular grid

1 Introduction

Research on numerical methods for solving convection-diffusion equations is of great importance since these equations are a basis for describing physical phenomena where particles, energy, or other physical quantities are transferred inside a physical system due to diffusion and convection processes. These equations are also used to describe advection-diffusion processes in

*Department of Mathematics, Faculty of Applied Science, King Mongkut's University of Technology North Bangkok, Bangkok, Thailand

[†]Université Paris-Est Marne-la-Vallée 5 boulevard Descartes Champs-sur-Marne F-77454 MARNE LA VALLÉE CEDEX 2, France

[‡]Department of Mechanical Engineering Technology, College of Industrial Technology, King Mongkut's University of Technology North Bangkok, Bangkok, Thailand

environmental science, e.g., pollutant transport in the atmosphere, oceans, rivers, or groundwater [25, 12, 5]. Convection is usually defined as the movement of a fluid due to heat, advection is usually defined as the movement of a substance due to the movement of a fluid transport medium, and diffusion refers to the dispersion of some substance through the physical domain of some other substance, e.g., the dispersion of a pollutant through a river. Generally, the scale of the diffusion is smaller by several orders of magnitude compared to the size of the advective flow field. The accurate simulation of such processes requires numerical methods that are able to compute if sharp layers exist without the occurrence of spurious oscillations.

Many methods have been proposed to overcome the instability and inaccuracy of numerical solutions of convection-diffusion equations. Methods which are usually used to solve convection-diffusion equations include the finite difference method, the finite element method, and the finite volume method. The principle of the finite difference method is to select some discretization points, then to assign one discrete unknown and write one equation per discretization point [18]. Also, the derivatives of the unknown are replaced by finite differences using a Taylor-series expansion. The finite difference method becomes difficult to use when the coefficients involved in the equation are discontinuous. For the finite element method, the domain of the convection-diffusion equation is discretized into a set of elements and the method of weighted residuals is usually applied to obtain a set of equations for each element, which are then assembled to form the system of equations. The solution at the element nodes are then obtained by solving the system of equations [19, 35]. The accuracy and the stability of this method needs to be further improved to achieve an accurate transient convection-diffusion solution [8]. For the finite volume method, the domain is discretized into a set of regions called control volumes. The divergence theorem is then applied to derive the system of equations. Higher-order temporal and spatial discretizations can also be used to obtain a more accurate solution. In the finite-volume method, discontinuities of coefficients are not a problem if the mesh is chosen so that the discontinuities of the coefficients occur on the boundaries of the control volumes [9].

In recent years, many researchers have used finite volume methods. Some examples of this research are as follows. In 2003, Aboubacar and Webster [1] proposed a cell-vertex hybrid finite volume-element method that is implemented on triangles and applied to the numerical solution of Oldroyd model fluids in contraction flows. They found that a linear finite volume stress representation with discontinuous stress gradients, and incorporating locally reduced quadrature at the re-entrant corner could enhance the stability properties of the numerical scheme. In 2006, Pudykiewicz [24] derived a finite volume algorithm for obtaining the solution of an advection-diffusion equation on a sphere based on the principle of semi-discretization. The monotonicity of the scheme was achieved with explicit adaptive dissipation. In 2008, Gao and Yuan [13] presented a characteristic finite volume element method for multiple space, nonlinear, convection-dominated diffusion problems. The calculus of variations, the commuting operator, and the theory of prior estimates was adopted in their proposed scheme. In 2011, Ten Thije Boonkamp and Anthonissen [28] proposed a finite volume scheme for advection-diffusion-reaction equations. Their scheme included a new integral representation for the flux of the one-dimensional advection-diffusion-reaction equation which was derived from the solution of a local boundary value problem for the entire equation including the source term. In 2012, Zhang et al. [34] presented a fourth-order finite volume method for solving the advection-diffusion equation with an AMR-enabled multigrid solver. The fourth-order Runge-Kutta method was used for the time

integration. The fourth-order accuracy was used to approximate face-averaged values from cell-averaged values. In 2013, Filimon et al. [10] proposed an iterated defect correction approach to achieve higher-order accuracy for the approximation of steady-state solutions. The scheme applied a posteriori to estimate the local discretization error of the lower-order finite volume scheme. This estimate was then used to iteratively shift the solution to higher-order accuracy by polynomial reconstruction. In 2013, Chen et al. [6] presented the concept of a two-grid finite volume element method combined with a modified method of characteristics for analyzing semi-linear, time-dependent, advection-dominated diffusion equations in two space dimensions. The solution of a nonlinear system on the fine-grid space was reduced to the solution of nonlinear and linear systems on the coarse-grid and the fine-grid, respectively. In 2014, Arachchige and Pettet [2] introduced a new method for numerically solving the advection-reaction-diffusion systems in one space dimension based on the usual finite volume method with a third order unwinding scheme for discretizing the advection term in space. A new linearization technique for the temporal integration of the nonlinear source terms was proposed to provide a very effective method in terms of computational cost for the simulations. In 2015, Liu et al. [17] applied a two-grid algorithm to decompose a nonlinear advection-dominated diffusion-reaction equation into a small nonlinear system on a coarse grid and a linear system on a fine grid, as previously proposed by Chen et al. [6]. The modified upwind finite volume element method was then used to approximate the solution of the systems. In 2016, Tambue [27] applied a finite volume method with a two-point flux approximation on regular meshes to solve an advection-diffusion-reaction problem with a nonlinear reaction term. Exponential time differencing of order one was then applied for temporal discretization. In 2017, Lin and Zhang [16] proposed a high-order finite-volume scheme for solving a steady-state advection-diffusion equation with nonlinear Robin boundary conditions. A generic algorithm for generating third-order, fourth-order, and even higher-order explicit ghost-filling formulas was used to enforce the nonlinear Robin boundary conditions in multiple dimensions under the framework of finite volume methods. In 2017, Yang and Tine [33] proposed a hybrid finite volume scheme where the construction of the numerical flux appeared as a combination of the WENO and Anti Dissipative Method fluxes for transport type equations. This property of the numerical flux is very suitable for deriving the long term asymptotic behavior of the solution of population dynamics models as previously shown in numerical simulations of polymerization/depolymerization type models. In 2018, Xu [32] proposed a modified finite volume method to solve convection-diffusion-reaction problems. The scheme was much more accurate and stable than the conventional finite volume method without widening the computational stencil. Some undetermined coefficients were introduced in discretizing the equation and then determined analytically by making the truncation error of the numerical scheme vanish and by expressing the higher order derivatives of the unknown function with lower order ones through the governing equation. Recently, Lan et al. [15] proposed a new positive finite volume scheme for two-dimensional convection-diffusion equations on deformed meshes. The convective flux was approximated using available information of the diffusive flux to keep the upwind property and obtain second-order accuracy. This method did not need to introduce any slope limiting technique.

The outline of this paper is as follows. In section 2, we summarize an explicit characteristic-based finite volume element method developed by Phongthanapanich and others that can provide stabilized numerical solutions for pure advection and advection-dominated diffusion prob-

lems [20, 13, 21, 22, 23]. The idea of this method is to derive a convection-diffusion equation along a characteristic path. The explicit cell-centered finite volume method is then employed to discretize this characteristic-based equation. The weighted residuals finite element method is then used to approximate cell-face gradient quantities. In Section 3, we analyze the convergence of the method for a one-dimensional example. In section 4, we examine the accuracy and robustness of four piecewise linear reconstruction techniques, e.g., Frink [11], Holmes-Connell [14], Green-Gauss [4], and least-squares methods [3] on structured triangular grids for three test cases. These cases consist of (1) mixing of hot with cold fronts [20, 29], (2) rotation of a Gaussian pulse [22], and (3) triangular wave flow [29]. Finally, in section 5, we give conclusions.

2 The Numerical Scheme

2.1 The characteristic unsteady convection-diffusion equation

The governing partial differential equation for the two-dimensional unsteady convection-diffusion problem is

$$\begin{aligned} \frac{\partial \phi}{\partial t} + \nabla \cdot (\mathbf{v}\phi - \varepsilon \nabla \phi) &= 0 \quad \text{in } \Omega \times T, \\ \phi(x, 0) &= \phi_0(x) \quad x \in \Omega, \Omega \subset \mathbb{R}^2, \end{aligned} \quad (1)$$

where ϕ is the scalar quantity, $\mathbf{v} = \mathbf{v}(\mathbf{x})$ is the given convection velocity vector, $\varepsilon \geq 0$ is the diffusion coefficient, and $t \in (0, T]$ for $T < \infty$. The boundary conditions are

$$\begin{aligned} \phi &= g_D \quad \text{in } \partial\Omega_D, \\ \varepsilon \frac{\partial \phi}{\partial \mathbf{n}} &= g_N \quad \text{in } \partial\Omega_N, \end{aligned} \quad (2)$$

with $\partial\Omega = \partial\Omega_D \cup \partial\Omega_N$ with $\partial\Omega_D \cup \partial\Omega_N = \emptyset$.

If a moving coordinate is assumed along the path of the characteristic wave, \mathbf{x}' with a speed of \mathbf{v} , the change of variable \mathbf{x} to \mathbf{x}' is expressed by $d\mathbf{x}' = d\mathbf{x} - \mathbf{v}dt$. By applying a characteristic approximation to trace advection in time as explained in Refs.[20, 22, 23] to Equation (1), we obtain

$$\frac{\partial \phi}{\partial t} - \nabla' \cdot (\varepsilon \nabla' \phi) = 0, \quad (3)$$

where all terms are to be evaluated at $\mathbf{x}' = \mathbf{x}'(t)$. We then discretize the time with time steps Δt and define $\phi^n = \phi(t^n)$, where $t^n = n\Delta t$, $n = 0, 1, 2, \dots$. Then, by carrying out a Taylor-series expansion, the convection term reappears in the equation along with an additional second-order term. This term acts as a smoothing operator that reduces the oscillations arising from the spatial discretization of the convection term. The fully explicit characteristic unsteady convection-diffusion equation is then given by

$$\phi^{n+1} - \phi^n = -\Delta t (\mathbf{v} \cdot \nabla \phi^n) + \varepsilon \nabla \cdot \nabla \phi^n + \frac{(\Delta t)^2}{2} \mathbf{v} \cdot \nabla (\mathbf{v} \cdot \nabla \phi^n). \quad (4)$$

Together with the use of the divergence-free assumption ($\nabla \cdot \mathbf{v} = 0$), Equation (4) can be written finally in the conservation form as

$$\phi^{n+1} - \phi^n = -\Delta t [\nabla \cdot (\mathbf{v}\phi^n - \varepsilon \nabla \phi^n)] + \frac{(\Delta t)^2}{2} \nabla \cdot [\mathbf{v} (\mathbf{v} \cdot \nabla \phi^n)]. \quad (5)$$

2.2 The finite volume method

The computational domain is first discretized into a collection of non-overlapping control volumes $\Omega_i = \Omega, i = 1, \dots, N$, that completely cover the domain such that $\Omega = \cup_{i=1}^N \Omega_i, \Omega_i \neq 0$ and $\Omega_i \cap \Omega_j = 0$ if $i \neq j$. To obtain the finite volume equation, Equation (5) is then integrated over the control volume Ω_i to yield

$$\int_{\Omega_i} (\phi^{n+1} - \phi^n) dA = \int_{\Omega_i} \left(-\Delta t [\nabla \cdot (\mathbf{v}\phi^n - \varepsilon \nabla \phi^n)] + \frac{(\Delta t)^2}{2} \nabla \cdot [\mathbf{v}(\mathbf{v} \cdot \nabla \phi^n)] \right) dA. \quad (6)$$

Then the divergence theorem is applied to the spatial terms to yield a fully explicit characteristic-based scheme for solving Equation (5) in the form

$$\phi_i^{n+1} = \phi_i^n - \frac{\Delta t}{|\Omega_i|} \sum_{j=1}^{N_f} |\Gamma_{ij}| \hat{\mathbf{n}}_{ij} \cdot \left[(\mathbf{v}_{ij}^n \phi_{ij}^n - \varepsilon \nabla \phi_{ij}^n) - \frac{\Delta t}{2} \mathbf{v}_{ij}^n (\mathbf{v}_i^n \cdot \nabla \phi_i^n) \right], \quad (7)$$

where N_f is the number of adjacent cell faces, $|\Omega_i|$ is the measure of Ω_i , Γ_{ij} is the segment of the boundary $\partial\Omega_i$ between the two adjacent control volumes Ω_i and Ω_j and $|\Gamma_{ij}|$ is the measure of Γ_{ij} . The quantities at the time t^n are defined by

$$\phi_i^n = \phi_i(t^n) = \frac{1}{|\Omega_i|} \int_{\Omega_i} \phi(\mathbf{x}, t^n) d\mathbf{x}, \quad (8)$$

and

$$\phi_{ij}^n = \phi_{ij}(t^n). \quad (9)$$

Finally, the scalar quantities at the cell faces, ϕ_{ij}^n , are approximated by applying a Taylor-series expansion in space such that

$$\phi_{ij}^n = \begin{cases} \phi_i^n + (\mathbf{x}_{ij} - \mathbf{x}_i) \cdot \nabla \phi_i^n, & \mathbf{v}_{ij}^n \cdot \hat{\mathbf{n}}_{ij} \geq 0 \\ \phi_j^n + (\mathbf{x}_{ij} - \mathbf{x}_j) \cdot \nabla \phi_j^n, & \text{otherwise} \end{cases}, \quad (10)$$

where \mathbf{v}_{ij}^n is the scaled normal velocity at Γ_{ij} , and $|\Gamma_{ij}^c|$ is the cell characteristic length. Moreover, the gradient term, $\nabla \phi_{ij}^n$, is approximated by the weighted residuals method which is commonly used in the finite element technique [29], and the time-step within each control volume i for Equation (7) is determined from

$$\Delta t = C \min_i \left(\frac{|\Omega_i|}{\max_{j=1, \dots, N_f} |\mathbf{v}_{ij}^n|}, \frac{|\Gamma_{ij}^c|^2}{2\varepsilon} \right), \quad (11)$$

where $0 < C \leq 1$.

The upwind schemes require flow states to be specified on the left and the right of a control surface. The first-order accurate spatial discretization gives a constant solution inside each control volume. The piecewise linear reconstruction must be applied to each control volume to achieve second-order accuracy. The main aim of this research is to compare the accuracy and robustness of four piecewise linear reconstruction techniques, e.g., Frink, Holmes-Connell, Green-Gauss, and least-squares methods for a computational domain discretized into a triangular grid.

Frink's linear-reconstruction method [11] can explicitly evaluate the gradient for a triangular grid due to the invariant geometric properties of the grid, e.g., a line from a node through the cell-centroid will intersect the midpoint of the opposite face, and the distance from the cell-centroid to the face-midpoint is one-third of the distance from the face-midpoint to the opposite node. The scalar values at the cell-face of two adjacent grids (ϕ_L, ϕ_R) are calculated by

$$\begin{aligned}\phi_L &= \phi_i + \frac{\Psi_i}{3} \left[\frac{(\phi_{i1} + \phi_{i2})}{2} - \phi_{i3} \right], \\ \phi_R &= \phi_j + \frac{\Psi_j}{3} \left[\frac{(\phi_{j1} + \phi_{j2})}{2} - \phi_{j3} \right],\end{aligned}\tag{12}$$

where ϕ_i and ϕ_j are assumed to be the solutions at the cell-centroids, ϕ_{ik}, ϕ_{jk} , where $k = 1, 2, 3$, are the solutions at the nodes of the left and right cells, respectively, and Ψ_i and Ψ_j are limiter functions [4, 30, 26]. The value at a node may be computed by inverse-distance weighting or by the pseudo-Laplacian method [11]. The inverse-distance weighting from a cell-centroid to the cell nodes that preserves the principle of positivity can be expressed as

$$\phi_n = \sum_{j=1}^{N_c} \frac{\phi_j}{|\mathbf{r}_j|} / \sum_{j=1}^{N_c} \frac{1}{|\mathbf{r}_j|},\tag{13}$$

where ϕ_j are the surrounding cell-centered values of the node n , $|\mathbf{r}_j|$ is the distance from the cell-centroid to node n , and N_c is the number of the surrounding cells. Otherwise, the pseudo-Laplacian method proposed by Holmes and Connell [14] can be used to determine nodal quantities such that

$$\phi_n = \sum_{j=1}^{N_c} (w_j \phi_j) / \sum_{j=1}^{N_c} \phi_j,\tag{14}$$

where the weights w_j are determined from

$$w_j = 1 + \lambda_x(x_j - x_n) + \lambda_y(y_j - y_n),\tag{15}$$

and the Lagrange multipliers, λ_x and λ_y are defined by

$$\begin{aligned}\lambda_x &= \frac{\sum_{j=1}^{N_c} (x_j - x_n)(y_j - y_n) \sum_{j=1}^{N_c} (y_j - y_n) - \sum_{j=1}^{N_c} (y_j - y_n)^2 \sum_{j=1}^{N_c} (x_j - x_n)}{\sum_{j=1}^{N_c} (x_j - x_n)^2 \sum_{j=1}^{N_c} (y_j - y_n)^2 - \left[\sum_{j=1}^{N_c} (x_j - x_n)(y_j - y_n) \right]^2}, \\ \lambda_y &= \frac{\sum_{j=1}^{N_c} (x_j - x_n)(y_j - y_n) \sum_{j=1}^{N_c} (x_j - x_n) - \sum_{j=1}^{N_c} (x_j - x_n)^2 \sum_{j=1}^{N_c} (y_j - y_n)}{\sum_{j=1}^{N_c} (x_j - x_n)^2 \sum_{j=1}^{N_c} (y_j - y_n)^2 - \left[\sum_{j=1}^{N_c} (x_j - x_n)(y_j - y_n) \right]^2}.\end{aligned}\tag{16}$$

The Green-Gauss approach [4] approximates the gradient of ϕ as the surface integral of the product of ϕ with an outward unit normal vector over a control volume such that

$$\nabla\phi = \frac{1}{\Omega} \int_{\partial\Omega} \phi \mathbf{n} dS. \quad (17)$$

For the center-centered scheme, the gradient at the center of cell i of the triangular grid [4] can be obtained from

$$\nabla\phi_i = \frac{1}{2\Omega} \sum_{k=1}^3 (\phi_i + \phi_k) \mathbf{n}_{ik} \Delta S_{ik}, \quad (18)$$

where the summation extends over all faces of the cell with volume Ω . The \mathbf{n}_{ik} is the outward unit normal vector and ΔS_{ik} is the k -face area of the cell i .

Lastly, the least-squares approach [3] is based on the use of a Taylor-series expansion for each edge which is incident to the cell-centered i . The linear reconstruction term along the common edge between control volume i and j can be computed as

$$\nabla\phi_i \cdot \mathbf{r}_{ij} = \phi_j - \phi_i, \quad (19)$$

where \mathbf{r}_{ij} is the vector from cell-centered i to j . By applying Equation (19) to three neighboring cells, we obtain the following system of linear equations

$$\begin{bmatrix} \Delta x_{i1} & \Delta y_{i1} \\ \Delta x_{i2} & \Delta y_{i2} \\ \Delta x_{i3} & \Delta y_{i3} \end{bmatrix} \begin{Bmatrix} \frac{\partial\phi_i}{\partial x} \\ \frac{\partial\phi_i}{\partial y} \end{Bmatrix} = \begin{Bmatrix} \phi_1 - \phi_i \\ \phi_2 - \phi_i \\ \phi_3 - \phi_i \end{Bmatrix}. \quad (20)$$

Finally, it is worth comparing the finite volume method (FVM) and discontinuous Galerkin method (DGM) concerning their efficiency. Moreover, DGM gives error estimates in stronger norms and with less regularity [7]. They are identical to finite volume schemes in the case of the formal first order (degree $k = 0$), and their computational costs are the same. However, for higher-order, DGM uses nonconformal ansatz functions whose restrictions to single cells are higher-degree polynomials. DGM with $k = 1$ may yield similar results as a piecewise linear reconstruction technique, but the effort for computing the fluxes for DGM is higher than for FVM.

3 Convergence of the characteristic finite volume method for one-dimensional convection

The analysis of the convergence of the scheme defined by (7) presents a few difficulties, that we analyse for the case of a one-dimensional problem and a non-uniform mesh. Let $\Omega = \mathbb{R}$. We intend to approximate the pure convection equation with a constant convection velocity $v > 0$,

$$\frac{\partial\phi}{\partial t} + \nabla \cdot (\mathbf{v}\phi) = \frac{\partial\phi}{\partial t} + v \frac{\partial\phi}{\partial x} = 0. \quad (21)$$

We remark that, defining $\phi_{\text{ini}}(x) = \phi(x, 0)$ for all $x \in \mathbb{R}$, the solution of (21) is given by $\phi(x, t) = \phi_{\text{ini}}(x - vt)$.

Although we don't include a diffusion term in the continuous equation, we include in the scheme a diffusion term, which is vanishing with the size of the mesh, and which plays a central role in the convergence proof. We assume that an increasing sequence $(x_{i+\frac{1}{2}})_{i \in \mathbb{Z}} \subset \mathbb{R}$ is given such that $\lim_{i \rightarrow \pm\infty} x_{i+\frac{1}{2}} = \pm\infty$, we define $h_i = x_{i+\frac{1}{2}} - x_{i-\frac{1}{2}}$. We assume that there exist $h > 0$, measuring the size of the mesh, and $\beta \in (1, +\infty)$, measuring the regularity of the mesh, such that

$$\beta h \geq h_i \geq \frac{1}{\beta} h \text{ for all } i \in \mathbb{Z}. \quad (22)$$

This means that the ratio of the sizes of any pair of control volumes is bounded by below and above. We then define the mesh $(\Omega_i)_{i \in \mathbb{Z}}$ by $\Omega_i = (x_{i-\frac{1}{2}}, x_{i+\frac{1}{2}})$. The center of gravity of Ω_i is $x_i = \frac{1}{2}(x_{i-\frac{1}{2}} + x_{i+\frac{1}{2}})$, and there holds $|\Omega_i| = h_i$. Then, for $i \in \mathbb{Z}$, we let $x_{ij} = x_{i \pm \frac{1}{2}}$ for $j = i \pm 1$. The initial condition is approximated by

$$\forall i \in \mathbb{Z}, \phi_i^0 = \phi_{\text{ini}}(x_i), \quad (23)$$

and Equation (7) becomes, in this 1D case,

$$\forall i \in \mathbb{Z}, \forall n \in \mathbb{N}, |\Omega_i| \frac{\phi_i^{n+1} - \phi_i^n}{\Delta t} + \sum_{j=i \pm 1} |\Gamma_{ij}| \hat{n}_{ij} \left(v_{ij}^n (\phi_{ij}^n - \frac{\Delta t v_i^n}{2} \nabla \phi_i^n) - \varepsilon \nabla \phi_{ij}^n \right) = 0. \quad (24)$$

with $|\Gamma_{ij}| = 1$, $v_{ij}^n = v$, $v_i^n = v$, $\hat{n}_{ij} = \pm 1$ for $j = i \pm 1$, and

$$\nabla \phi_i^n := \frac{\phi_{i+1}^n - \phi_{i-1}^n}{x_{i+1} - x_{i-1}}, \quad \nabla \phi_{ij}^n := \frac{\phi_j^n - \phi_i^n}{x_j - x_i}.$$

The vanishing diffusion term is defined by $\varepsilon = v\beta h$. For $j = i + 1$, using the fact that the unwinding direction is from i to $i + 1$, we can write

$$\phi_{ij}^n = \phi_i^n + (x_{ij} - x_i) \nabla \phi_i^n = \phi_i^n + \frac{h_i}{2} \frac{\phi_{i+1}^n - \phi_{i-1}^n}{x_{i+1} - x_{i-1}}.$$

We then set

$$\phi_{i+\frac{1}{2}}^n := \phi_{ij}^n - \frac{\Delta t v}{2} \nabla \phi_i^n - \frac{\varepsilon}{v} \nabla \phi_{ij}^n = \phi_i^n + \alpha_i (\phi_{i+1}^n - \phi_{i-1}^n) + \theta_{i+\frac{1}{2}} (\phi_i^n - \phi_{i+1}^n), \quad (25)$$

with $\alpha_i = \frac{h_i - \Delta t v}{2(x_{i+1} - x_{i-1})}$ and $\theta_{i+\frac{1}{2}} = \frac{\beta h}{x_{i+1} - x_i}$. In the following, we will assume that

$$v \Delta t \leq C_{\text{cfl}} h, \quad (26)$$

for the value C_{cfl} (which only depends on β) defined below in (34). Using $C_{\text{cfl}} \leq \frac{1}{\beta}$, $x_{i+1} - x_i = \frac{1}{2}(h_i + h_{i+1})$ and $x_{i+1} - x_{i-1} = \frac{1}{2}(h_{i-1} + h_{i+1}) + h_i$, we obtain

$$0 \leq \alpha_i \leq \frac{1}{2} \text{ and } 1 \leq \theta_{i+\frac{1}{2}} \leq \beta^2. \quad (27)$$

From (25) and (24), we get

$$\forall i \in \mathbb{Z}, \forall n \in \mathbb{N}, h_i \frac{\phi_i^{n+1} - \phi_i^n}{\Delta t} + v(\phi_{i+\frac{1}{2}}^n - \phi_{i-\frac{1}{2}}^n) = 0. \quad (28)$$

Note that (28) makes clear the finite volume structure of Scheme (24) and that, due to the negative coefficient in the dependence of $\phi_{i-\frac{1}{2}}^n$ with respect to ϕ_{i-2}^n , no L^∞ bound can be proved on the scheme.

We can state the following convergence result.

Theorem 3.1 *Let us assume that, letting ϕ be the solution to (21) and defining $\phi_{\text{ini}}(x) = \phi(x, 0)$ for all $x \in \mathbb{R}$, the function $\phi_{\text{ini}} \in C^2(\mathbb{R})$ has a compact support. Let $T > 0$ and $\beta \in (1, +\infty)$ be given, and let $h \in (0, 1)$ and $N \in \mathbb{N}^*$ be given such that $\Delta t = T/N$ satisfies (26) where C_{cf} is defined by (34). For a given mesh defined as above, and satisfying (22), let ϕ_i^n , for all $i \in \mathbb{Z}$ and $n \in \mathbb{N}$, be the solution of Scheme (23), (25) and (28). Then there exists $C > 0$, only depending on T , v , ϕ_{ini} and β such that*

$$\|e^N\|_{L^2} \leq Ch, \quad (29)$$

where $\|e^N\|_{L^2}$, the approximate L^2 norm of the error at time T , is defined by

$$\|e^N\|_{L^2}^2 = \sum_{i \in \mathbb{Z}} h_i (\phi_i^N - \phi(x_i, T))^2.$$

PROOF

Let us compute the consistency error, obtained by replacing ϕ_i^n in the scheme by $\widehat{\phi}_i^n := \phi(x_i, n\Delta t)$. We obtain

$$\forall i \in \mathbb{Z}, \forall n \in \mathbb{N}, h_i \frac{\widehat{\phi}_i^{n+1} - \widehat{\phi}_i^n}{\Delta t} + v(\widehat{\phi}_{i+\frac{1}{2}}^n - \widehat{\phi}_{i-\frac{1}{2}}^n) = v h_i R_i^n, \quad (30)$$

with

$$\widehat{\phi}_{i+\frac{1}{2}}^n = \widehat{\phi}_i^n + \alpha_i (\widehat{\phi}_{i+1}^n - \widehat{\phi}_{i-1}^n) + \theta_{i+\frac{1}{2}} (\widehat{\phi}_i^n - \widehat{\phi}_{i+1}^n), \quad \widehat{\phi}_{i-\frac{1}{2}}^n = \widehat{\phi}_{i-1}^n + \alpha_{i-1} (\widehat{\phi}_i^n - \widehat{\phi}_{i-2}^n) + \theta_{i-\frac{1}{2}} (\widehat{\phi}_{i-1}^n - \widehat{\phi}_i^n).$$

Expressing $\widehat{\phi}_j^n = \phi_{\text{ini}}(x_j - vn\Delta t)$, for any $j = i - 2, \dots, i + 1$, as a Taylor expansion from $x_{i,0} = x_i - vn\Delta t$, we find that

$$\widehat{\phi}_{i+\frac{1}{2}}^n = \phi_{\text{ini}}(x_{i,0}) + \left(\frac{1}{2}(h_i - \Delta t v) - \beta h\right) \phi'_{\text{ini}}(x_{i,0}) + h_i R_{i,+}^n$$

and

$$\widehat{\phi}_{i-\frac{1}{2}}^n = \phi_{\text{ini}}(x_{i,0}) + \left(\frac{1}{2}(-h_i - \Delta t v) - \beta h\right) \phi'_{\text{ini}}(x_{i,0}) + h_i R_{i,-}^n,$$

with

$$\forall i \in \mathbb{Z}, \forall n \in \mathbb{N}, |R_{i,\pm}^n| \leq C_{0,x} h,$$

for some $C_{0,x} > 0$, depending only on a bound of $|\phi''_{\text{ini}}|$, on v and on β . This leads to

$$v(\widehat{\phi}_{i+\frac{1}{2}}^n - \widehat{\phi}_{i-\frac{1}{2}}^n) = h_i v (\phi'_{\text{ini}}(x_{i,0}) + R_{i,+}^n - R_{i,-}^n).$$

We have

$$\frac{\widehat{\phi}_i^{n+1} - \widehat{\phi}_i^n}{\Delta t} = -v\phi'_{\text{ini}}(x_{i,0}) + vR_i^{n,+},$$

with

$$\forall i \in \mathbb{Z}, \forall n \in \mathbb{N}, |R_i^{n,+}| \leq C_{0,t}\Delta t,$$

for some $C_{0,t} > 0$, depending only on a bound of $|\phi''_{\text{ini}}|$ and on v . Gathering the above results, we get that there exists $C_0 > 0$, depending only on a bound of $|\phi''_{\text{ini}}|$, on v and on β , such that

$$\forall i \in \mathbb{Z}, \forall n \in \mathbb{N}, |R_i^n| \leq C_0 h.$$

Accounting for the fact that the support of ϕ_{ini} is compact, and assuming that $h \leq 1$, we get that there exists $C_1 > 0$, only depending on a bound of $|\phi''_{\text{ini}}|$, on the support of ϕ_{ini} , on v and on β , such that

$$\forall n \in \mathbb{N}, \sum_{i \in \mathbb{Z}} h_i (R_i^n)^2 \leq C_1 h^2. \quad (31)$$

We then denote $e_i^n = \widehat{\phi}_i^n - \phi_i^n$, and we obtain, by subtracting (28) from (30),

$$\forall i \in \mathbb{Z}, \forall n \in \mathbb{N}, h_i \frac{e_i^{n+1} - e_i^n}{\Delta t} + v(e_{i+\frac{1}{2}}^n - e_{i-\frac{1}{2}}^n) = v h_i R_i^n, \quad (32)$$

with

$$e_{i+\frac{1}{2}}^n = e_i^n + \alpha_i(e_{i+1}^n - e_{i-1}^n) + \theta_{i+\frac{1}{2}}(e_i^n - e_{i+1}^n), \quad e_{i-\frac{1}{2}}^n = e_{i-1}^n + \alpha_{i-1}(e_i^n - e_{i-2}^n) + \theta_{i-\frac{1}{2}}(e_{i-1}^n - e_i^n),$$

and

$$\forall i \in \mathbb{Z}, e_i^0 = 0. \quad (33)$$

Let us notice that, due to the compact support assumption, for any $n \in \mathbb{N}$, the number of $i \in \mathbb{Z}$ such that $e_i^n \neq 0$ or $R_i^n \neq 0$ is finite. We multiply (32) by $\Delta t e_i^n$, and we sum on $i \in \mathbb{Z}$ and on $n = 0, \dots, N-1$. This leads to $T_1 + T_2 = T_3$ with

$$T_1 = \sum_{n=0}^{N-1} \sum_{i \in \mathbb{Z}} h_i (e_i^{n+1} - e_i^n) e_i^n,$$

$$T_2 = \Delta t v \sum_{n=0}^{N-1} \sum_{i \in \mathbb{Z}} (e_{i+\frac{1}{2}}^n - e_{i-\frac{1}{2}}^n) e_i^n,$$

and

$$T_3 = \Delta t v \sum_{n=0}^{N-1} \sum_{i \in \mathbb{Z}} h_i e_i^n R_i^n.$$

We have, thanks to a discrete integration by parts, that

$$T_2 = \Delta t v \sum_{n=0}^{N-1} \sum_{i \in \mathbb{Z}} e_{i+\frac{1}{2}}^n (e_i^n - e_{i+1}^n).$$

Since there holds

$$e_i^n(e_i^n - e_{i+1}^n) = \frac{1}{2}(e_i^n)^2 - \frac{1}{2}(e_{i+1}^n)^2 + \frac{1}{2}(e_i^n - e_{i+1}^n)^2,$$

we get

$$T_2 = \Delta t v \sum_{n=0}^{N-1} \sum_{i \in \mathbb{Z}} \left(\left(\frac{1}{2} + \theta_{i+\frac{1}{2}} - \alpha_i \right) (e_i^n - e_{i+1}^n)^2 + \alpha_i (e_i^n - e_{i-1}^n) (e_i^n - e_{i+1}^n) \right).$$

Using the inequality

$$(e_i^n - e_{i-1}^n)(e_i^n - e_{i+1}^n) \geq -\frac{1}{2}((e_i^n - e_{i-1}^n)^2 + (e_i^n - e_{i+1}^n)^2),$$

we obtain, using (27),

$$T_2 \geq \Delta t v \sum_{n=0}^{N-1} \sum_{i \in \mathbb{Z}} \left(\frac{1}{2} + \theta_{i+\frac{1}{2}} - \alpha_i - \frac{1}{2}(\alpha_i + \alpha_{i+1}) \right) (e_i^n - e_{i+1}^n)^2 \geq \frac{1}{2} \Delta t v \sum_{n=0}^{N-1} \sum_{i \in \mathbb{Z}} (e_i^n - e_{i+1}^n)^2.$$

Using the relation

$$(e_i^{n+1} - e_i^n) e_i^n = \frac{1}{2}(e_i^{n+1})^2 - \frac{1}{2}(e_i^n)^2 - \frac{1}{2}(e_i^{n+1} - e_i^n)^2,$$

we get

$$T_1 = \sum_{i \in \mathbb{Z}} \frac{h_i}{2} (e_i^N)^2 - \sum_{n=0}^{N-1} \sum_{i \in \mathbb{Z}} \frac{h_i}{2} (e_i^{n+1} - e_i^n)^2.$$

We now use (32) and (27). We get

$$h_i |e_i^{n+1} - e_i^n| \leq v \Delta t \left(\beta^2 |e_i^n - e_{i+1}^n| + \left(\frac{3}{2} + \beta^2 \right) |e_i^n - e_{i-1}^n| + \frac{1}{2} |e_{i-1}^n - e_{i-2}^n| + h_i |R_i^n| \right).$$

Applying the Cauchy-Schwarz inequality, we obtain

$$\begin{aligned} -h_i (e_i^{n+1} - e_i^n)^2 &\geq -\frac{v^2 \Delta t^2}{h_i} (2 + 2\beta^2 + h_i) \\ &\quad \times \left(\beta^2 (e_i^n - e_{i+1}^n)^2 + \left(\frac{3}{2} + \beta^2 \right) (e_i^n - e_{i-1}^n)^2 + \frac{1}{2} (e_{i-1}^n - e_{i-2}^n)^2 + h_i (R_i^n)^2 \right). \end{aligned}$$

This yields, under the condition $h < 1$,

$$T_1 \geq \sum_{i \in \mathbb{Z}} \frac{h_i}{2} (e_i^N)^2 - \frac{\beta v^2 \Delta t^2}{2h} (2 + 2\beta^2 + \beta) \left((2 + 2\beta^2) \sum_{n=0}^{N-1} \sum_{i \in \mathbb{Z}} (e_i^n - e_{i+1}^n)^2 + \sum_{n=0}^{N-1} \sum_{i \in \mathbb{Z}} h_i (R_i^n)^2 \right).$$

We now choose C_{eff} in (26) such that the terms in $(e_i^n - e_{i+1}^n)^2$ in $T_1 + T_2$ are non-negative. Indeed, there holds

$$\frac{v \Delta t}{2} - \frac{\beta v^2 \Delta t^2}{2h} (2 + 2\beta^2 + \beta) (2 + 2\beta^2) \geq 0,$$

under condition (26), provided that

$$C_{\text{cfl}} = \frac{1}{\beta(2 + 2\beta^2 + \beta)(2 + 2\beta^2)} \text{ which is such that } C_{\text{cfl}} < \frac{1}{\beta}. \quad (34)$$

We thus obtain the existence of C_2 , only depending on β such that

$$T_1 + T_2 \geq \sum_{i \in \mathbb{Z}} \frac{h_i}{2} (e_i^N)^2 - C_2 v \Delta t \sum_{n=0}^{N-1} \sum_{i \in \mathbb{Z}} h_i (R_i^n)^2.$$

Gathering the above relations, we obtain

$$\sum_{i \in \mathbb{Z}} \frac{h_i}{2} (e_i^N)^2 - C_2 v \Delta t \sum_{n=0}^{N-1} \sum_{i \in \mathbb{Z}} h_i (R_i^n)^2 \leq v \Delta t \sum_{n=0}^{N-1} \sum_{i \in \mathbb{Z}} h_i |e_i^n| |R_i^n|.$$

We apply the inequality $ab \leq \frac{1}{2}(a^2 + b^2)$ to the right-hand-side of the above inequality, and we multiply by 2, which yields

$$\sum_{i \in \mathbb{Z}} h_i (e_i^N)^2 \leq v \Delta t \sum_{n=0}^{N-1} \sum_{i \in \mathbb{Z}} h_i (e_i^n)^2 + (1 + 2C_2) v \Delta t \sum_{n=0}^{N-1} \sum_{i \in \mathbb{Z}} h_i (R_i^n)^2.$$

Applying (31), we deduce

$$\sum_{i \in \mathbb{Z}} h_i (e_i^N)^2 \leq v \Delta t \sum_{n=0}^{N-1} \sum_{i \in \mathbb{Z}} h_i (e_i^n)^2 + (1 + 2C_2) v T C_1 h^2.$$

We remark that all the preceding inequalities hold, replacing N by any value in $\{1, \dots, N\}$. Therefore we can apply Lemma 3.1, and we obtain

$$\sum_{i \in \mathbb{Z}} h_i (e_i^N)^2 \leq e^{vT} (1 + 2C_2) v T C_1 h^2.$$

This proves (29), and concludes the proof of the theorem.

Theorem 3.1 (Discrete Gronwall lemma) *Let $N \in \mathbb{N}^*$, $T > 0$ and $\Delta t = T/N$. Let $b \geq 0$ and $v > 0$ be given, and let $(a_n)_{n=0, \dots, N}$ be non-negative real values with $a_0 = 0$ and*

$$a_n \leq v \Delta t \sum_{k=0}^{n-1} a_k + b \text{ for } n \in \{0, \dots, N\}$$

Then

$$a_N \leq b e^{vT}.$$

PROOF

We set $A_n = \sum_{k=0}^{n-1} a_k$ for $n = 1, \dots, N$ and $A_0 = 0$. We then have

$$A_n - A_{n-1} \leq v \Delta t A_{n-1} + b,$$

and therefore $A_n \leq (1 + v \Delta t)^n A_0 + \frac{b((1 + v \Delta t)^n - 1)}{1 + v \Delta t - 1} = \frac{b((1 + v \Delta t)^n - 1)}{v \Delta t} \leq \frac{b(e^{vT} - 1)}{v \Delta t}$ since $A_0 = 0$ (recall that $(1 + \frac{x}{N})^n \leq e^x$ for $x \geq 0$ and $n \leq N$). This finally leads to

$$a_N \leq v \Delta t A_N + b \leq b(e^{vT} - 1) + b = b e^{vT}.$$

4 Test Problems

In this section, three examples of pure convection and convection-dominated diffusion problems are examined to evaluate the accuracy and robustness of four piecewise linear reconstruction methods. These examples are (1) the mixing of hot with cold fronts, (2) the rotation of a Gaussian pulse, and (3) triangular wave flow. All examples in this section were tested on structured triangular grids. For all numerical solutions, we use a triangular grid discretization of the domain, and assume that the limiter function $\Psi = 1$ (equation (12)).

4.1 Mixing of hot with cold fronts

The first example is a pure-convection problem of the mixing of hot with a cold fronts [20, 29]. The computational domain is $\Omega = (-4, -4) \times (4, 4)$ and the velocity field is given by

$$\mathbf{v} = -\frac{y}{r} \frac{f_t}{0.385} \mathbf{i} + \frac{x}{r} \frac{f_t}{0.385} \mathbf{j}, \quad (35)$$

where $r = \sqrt{x^2 + y^2}$ is the distance from the origin and $f_t = \frac{\tanh(r)}{\cosh^2(r)}$. The initial condition is specified by

$$\phi_0(\mathbf{x}) = -\tanh\left(\frac{y}{2}\right). \quad (36)$$

The exact solution is

$$\phi(\mathbf{x}, t) = -\tanh\left(\frac{y}{2} \cos\left(\frac{f_t}{0.385r}t\right) - \frac{x}{2} \sin\left(\frac{f_t}{0.385r}t\right)\right). \quad (37)$$

The 2D and 3D plots of the exact solution at the final time $t = 4$ are shown in Figures 1 and 2, respectively. The corresponding numerical solutions obtained from the three uniform grids S1 (16×16), S2 (32×32), and S3 (64×64) compared to the exact solution along the line $y = 0$ are depicted in Figures 3- 5, respectively. The L_2 -norm error of the solutions obtained by using four piecewise linear reconstruction techniques are shown in Table 1. We can see that the Frink and Holmes-Connell methods gave the most accurate solutions on grids S1 and S2, while the least-squares method gave the most accurate solution on grid S3. The Green-Gauss method gave the worst solution on all grid sizes.

Table 1: Comparison of L_2 -norm errors for problem 4.1.

$\ e\ _{L_2}$	S1	S2	S3
Frink	0.004848248	0.001285789	0.0002236133
Holmes-Connell	0.004848264	0.001285792	0.0002236136
Green-Gauss	0.005117222	0.001370439	0.0002785007
Least-Squares	0.004879665	0.001295393	0.0002080393

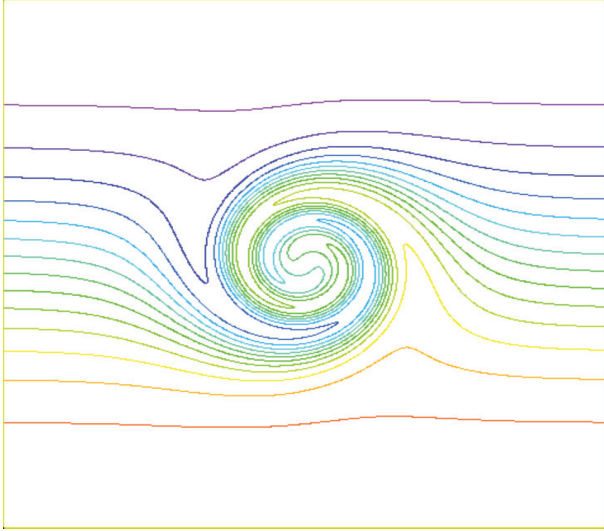


Figure 1: Exact solution at the final time of problem 4.1: 2D plot.

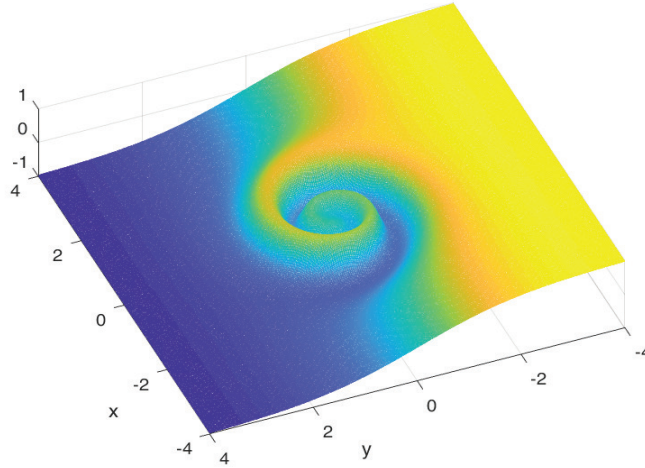


Figure 2: Exact solution at the final time of problem 4.1: 3D plot.

4.2 Rotation of Gaussian pulse

The second example is the rotation of a Gaussian pulse around the domain $\Omega = (-0.5, -0.5) \times (0.5, 0.5)$. We started the test using the pure convection problem with the initial condition $\phi(\mathbf{x}, 0)$ given as [22]

$$\phi(\mathbf{x}, 0) = \exp\left(-\frac{(x - x_c)^2 + (y - y_c)^2}{2\sigma^2}\right), \quad (38)$$

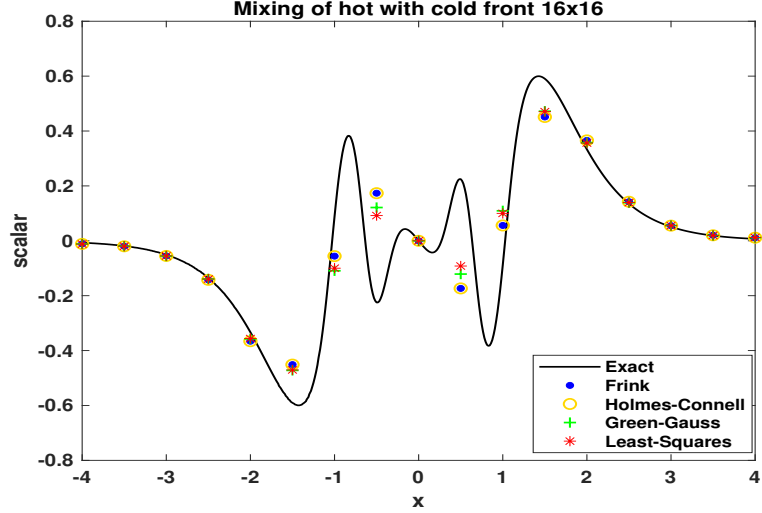


Figure 3: Comparison of the solutions of problem 4.1 on grid S1

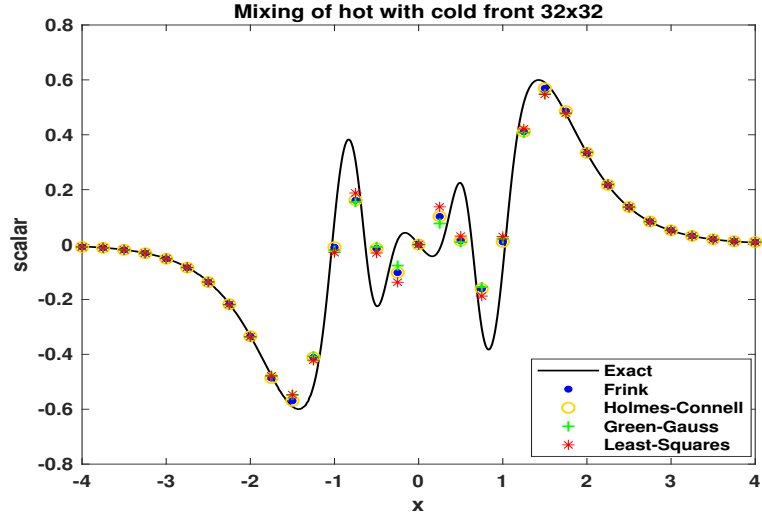


Figure 4: Comparison of the solutions of problem 4.1 on grid S2

where $(x_c, y_c) = (-0.25, 0)$ and $\sigma = 0.0447$ are the center coordinates and the standard deviation, respectively. The rotating velocity field $\mathbf{v}(\mathbf{x})$, with the angular velocity of 4 rad/s is given by

$$u(\mathbf{x}) = -4y \quad \text{and} \quad v(\mathbf{x}) = 4x. \quad (39)$$

The 2D and 3D plots of the exact solution at the final time $t = \pi/2$ are shown in Figures 6 and 7, respectively. The comparison between exact and numerical solutions obtained from the grids S2, S3, and S4 (128×128) along the line $y = 0$ are illustrated in Figures 8- 10, respectively. The comparison of the L_2 -norm errors in the solutions is given in Table 2. We may conclude that

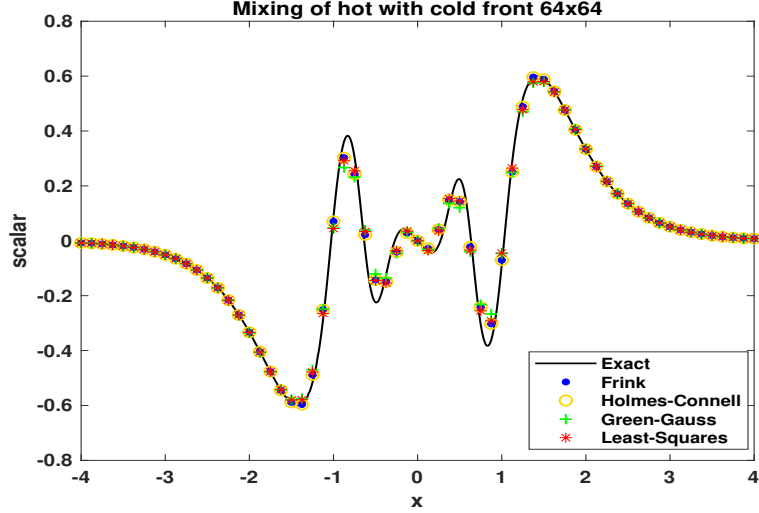


Figure 5: Comparison of the solutions of problem 4.1 on grid S3

the last-squares method gave the most accurate solution and the Green-Gauss method gave the least accurate solution. On grid S4, the L_2 -norm error value of the solution obtained using the least-square methods is about 100% better than the Frink and the Holmes-Connell methods, and 440% better than the Green-Gauss method.

Table 2: Comparison of the L_2 -norm errors for problem 4.2: Pure convection.

$\ e\ _{L_2}$	S2	S3	S4
Frink	0.001100730	0.0002354509	0.00003324699
Holmes-Connell	0.001100731	0.0002354509	0.00003324699
Green-Gauss	0.001080318	0.0002938341	0.00007430981
Least-Squares	0.0008085976	0.0001357213	0.00001689011

This example is repeated again as a convection-dominated diffusion problem by setting the diffusion coefficient of $\epsilon = 10^{-4}$. The exact solution of this test at the same final time is determined by [31, 22] as

$$\phi(\mathbf{x}, 0) = \frac{2\sigma^2}{2\sigma^2 + 4t\epsilon} \exp\left(-\frac{(x - x_c)^2 + (y - y_c)^2}{2\sigma^2 + 4t\epsilon}\right). \quad (40)$$

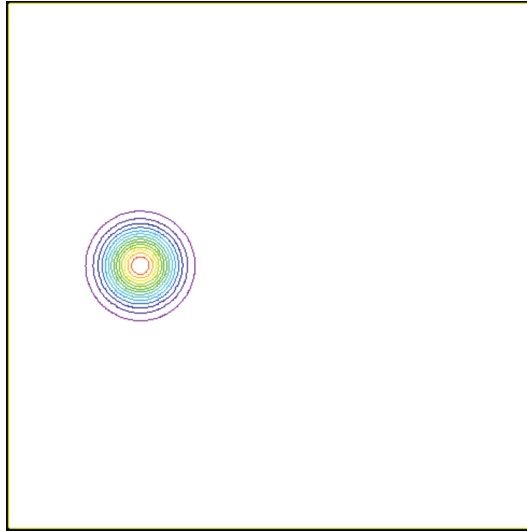


Figure 6: 2D plot of the exact solution at the final time of problem 4.2: Pure convection.

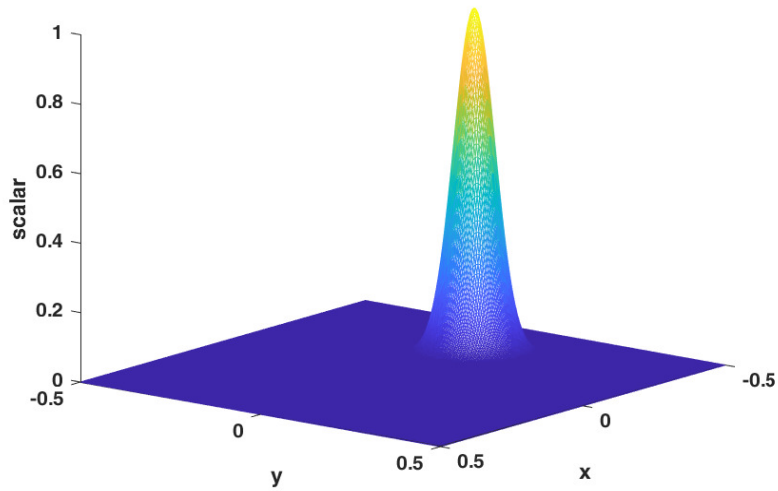


Figure 7: 3D plot of the exact solution at the final time of problem 4.2: Pure convection.

The 2D and 3D plots of the exact solution, are shown in Figures 11 and 12, respectively. The comparison between exact and numerical solutions obtained from the grids S2, S3 and S4 are illustrated in Figures 13- 15. The comparison of the L_2 -norm errors, are shown in Table 3. As we found for the pure convection case, the least-squares method gave the most accurate solution for all grids. On grid S4, the L_2 -norm error values of the solutions obtained by the least-squares method is about 123% better than the Frink and the Holmes-Connell methods, and 530% better than the Green-Gauss method. Finally, we note that the Frink and the Holmes-Connell methods

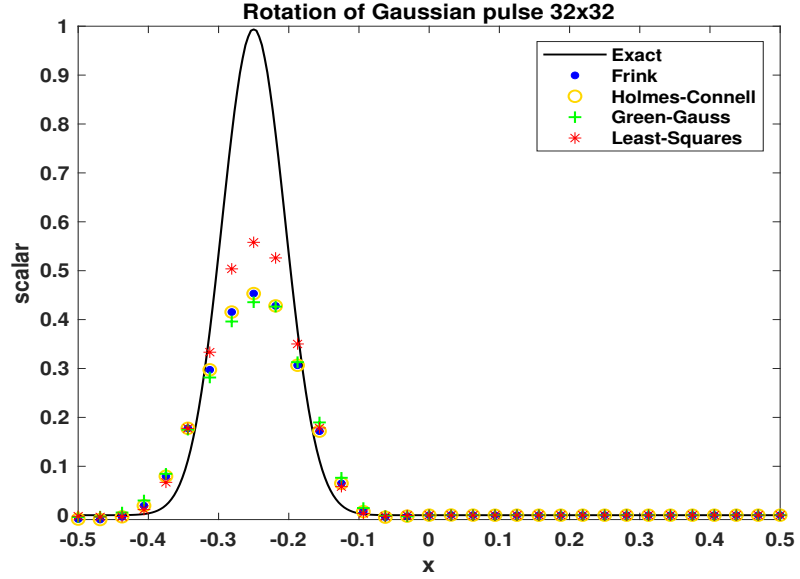


Figure 8: Comparison of the solutions of problem 4.2 on grid S2: Pure convection.

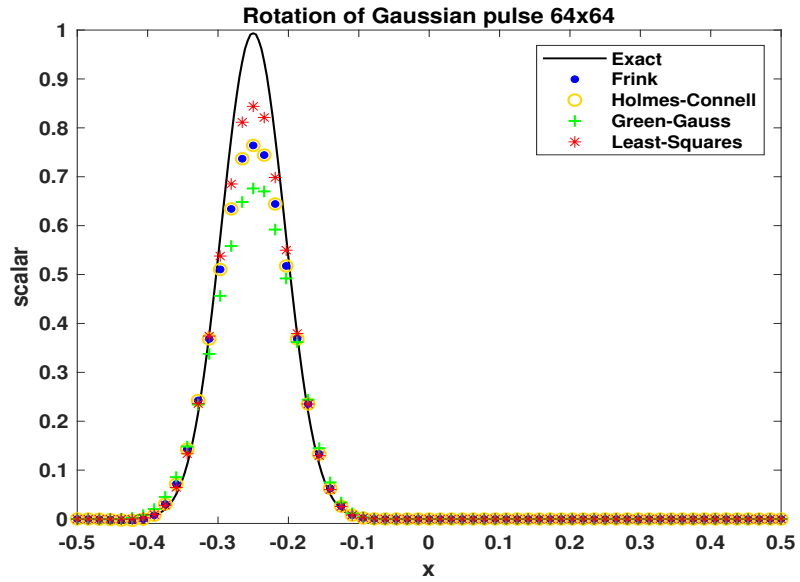


Figure 9: Comparison of the solutions of problem 4.2 on grid S3: Pure convection.

gave the same L_2 -norm errors for these tests.

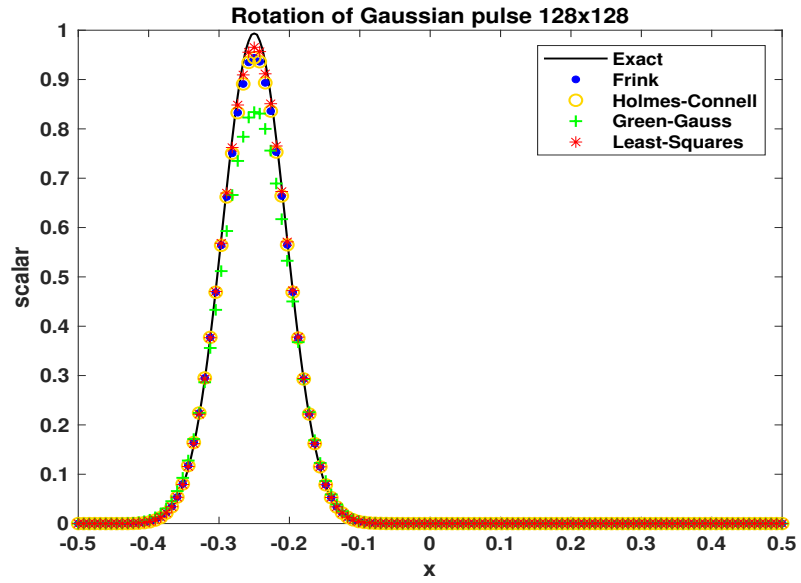


Figure 10: Comparison of the solutions of problem 4.2 on grid S4: Pure convection.

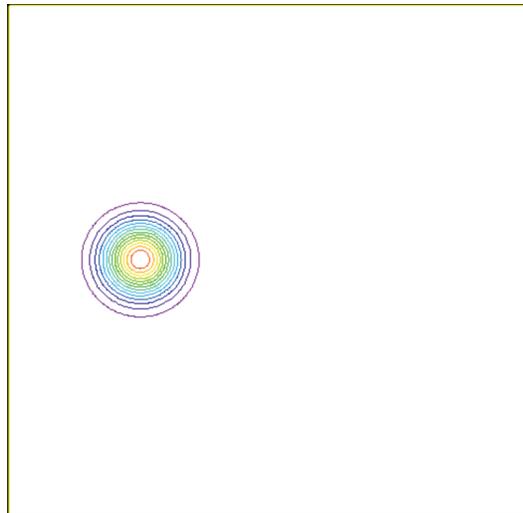


Figure 11: 2D plot of the exact solution at the final time of problem 4.2: Convection-Diffusion.

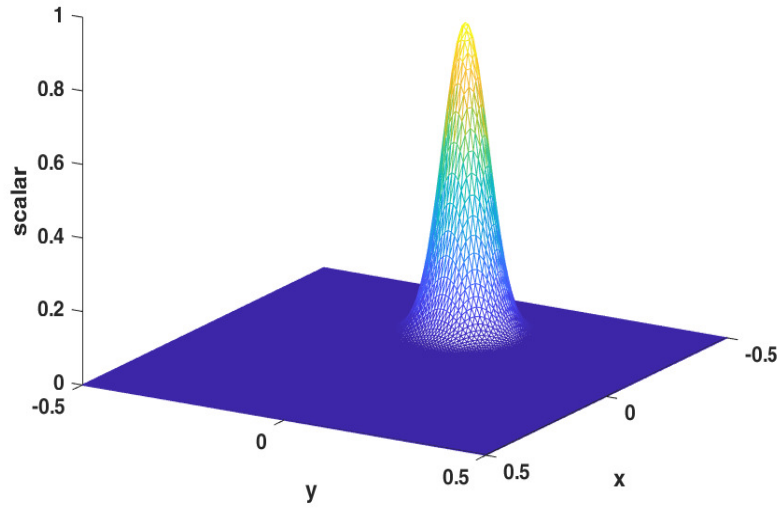


Figure 12: 3D plot of the exact solution at the final time of problem 4.2: Convection-Diffusion.

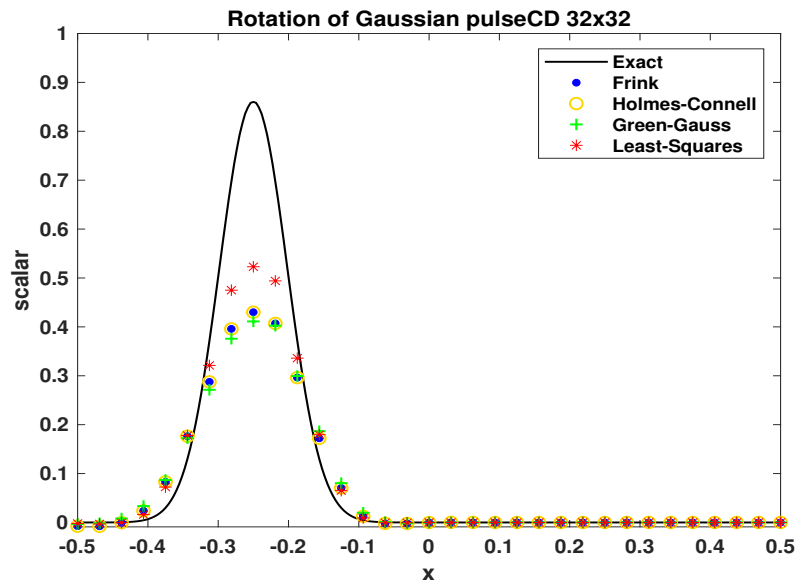


Figure 13: Comparison of the solutions of problem 4.2 on grid S2: Convection-Diffusion.

4.3 Triangular wave flow

The last example is the so-called triangular wave flow problem [29]. This is a pure-convection problem with an initial discontinuous flow profile. The computational domain is a unit square

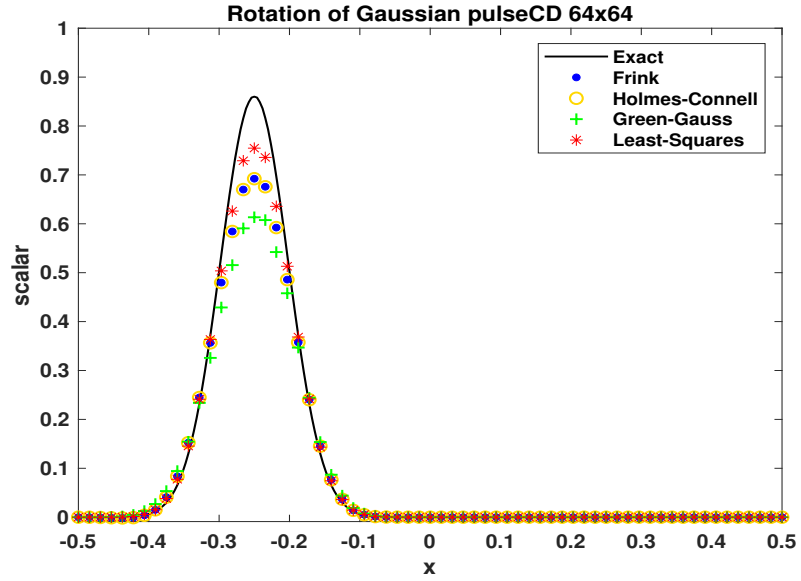


Figure 14: Comparison of the solutions of problem 4.2 on grid S3: Convection-Diffusion.

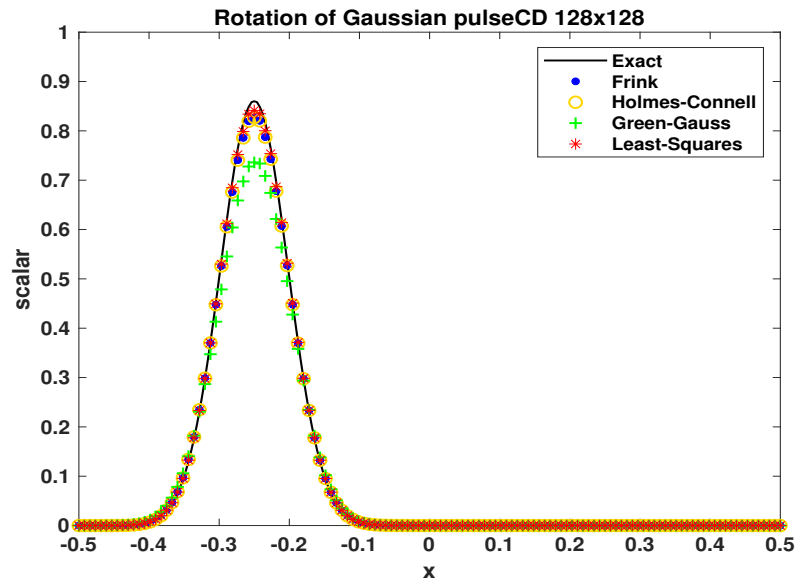


Figure 15: Comparison of the solutions of problem 4.2 on grid S4: Convection-Diffusion.

of $\Omega = (0, 1) \times (0, 1)$. For the initial condition, $\phi_0(\mathbf{x})$ is set to zero. The boundary conditions at

Table 3: Comparison of L_2 -norm errors for problem 4.2: Convection-Diffusion.

$\ e\ _{L_2}$	S2	S3	S4
Frink	0.0009283025	0.0001863148	0.00002602896
Holmes-Connell	0.0009283033	0.0001863148	0.00002602896
Green-Gauss	0.0009172858	0.0002428729	0.00006169527
Least-Squares	0.0006557170	0.0001008259	0.00001165540

$t = 0$ are prescribed by

$$\phi(0, y) = \begin{cases} 2(y - 0.25), & 0.25 \leq y \leq 0.50 \\ 2(0.75 - y), & 0.50 \leq y \leq 0.75 \\ 0, & \text{otherwise} \end{cases} \quad (41)$$

The velocity field is given by $\mathbf{v} = 0.05\mathbf{i}$.

This example is used to evaluate the robustness of the piecewise linear reconstruction techniques against the scalar discontinuity on four grids (S1,S2,S3,S4). For the coarse grid S1 (Figure 16), all methods gave nearly identical solutions without oscillation. For grid size S2, a slight oscillation occurs as shown in Figure 17. For S2, the Frink and the Holmes-Connell methods gave identical solutions along the line $y = 0.5$ with relatively small oscillations, while the solutions for the Green-Gauss and the least-squares methods gave larger oscillations. For the finer grids S3 and S4, the oscillations were appreciably larger as shown in Figures 18 and 19. Finally, the results in Figures 18 and 19 show that the Frink and the Holmes-Connell methods gave oscillating solutions downstream of the discontinuity while the Green-Gauss and the least-squares gave an oscillating solution upstream of the discontinuity.

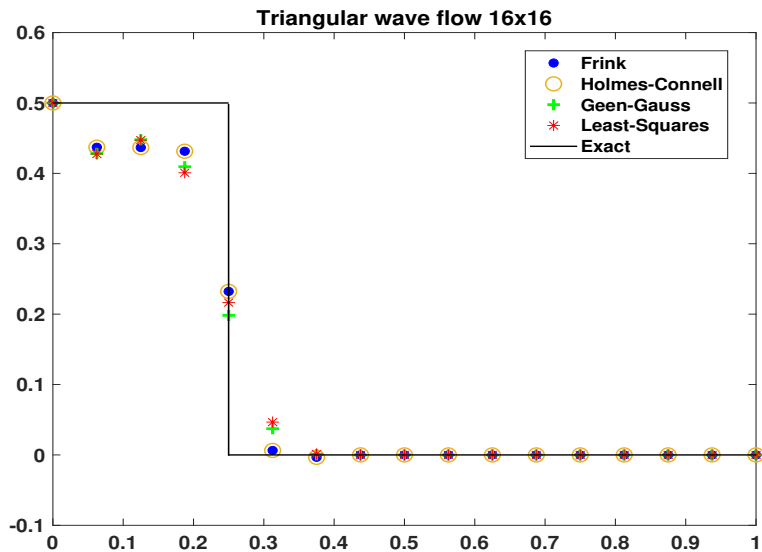


Figure 16: Comparison of the solutions of problem 4.3 on grid S1.

Acknowledgments

The first author is pleased to acknowledge the Science Achievement Scholarship of Thailand (SAST) for supporting this research work.

5 Conclusions

This paper presents an explicit characteristic finite volume method for solving the convection-diffusion equation in a two-dimensional domain. The method combines the characteristic-based scheme developed for the finite element method with the finite volume method for deriving the discretized equations from the convection-diffusion equation. The convergence of numerical solutions of the finite volume equations has been studied for four piecewise linear reconstruction techniques, namely, Frink [11], Holmes-Connell [14], Green-Gauss [4], and least-squares [3]. An analysis of the convergence of the scheme for a one-dimensional problem has been given in Section 3. The accuracy and robustness of the four linear construction techniques has been tested on three examples, namely, mixing of hot with cold fronts [20, 29], rotation of a Gaussian pulse [22] and triangular wave flow [29], for the special case of a triangular grid discretization of the domain. It was found that the least-squares method provided the most accurate solution for

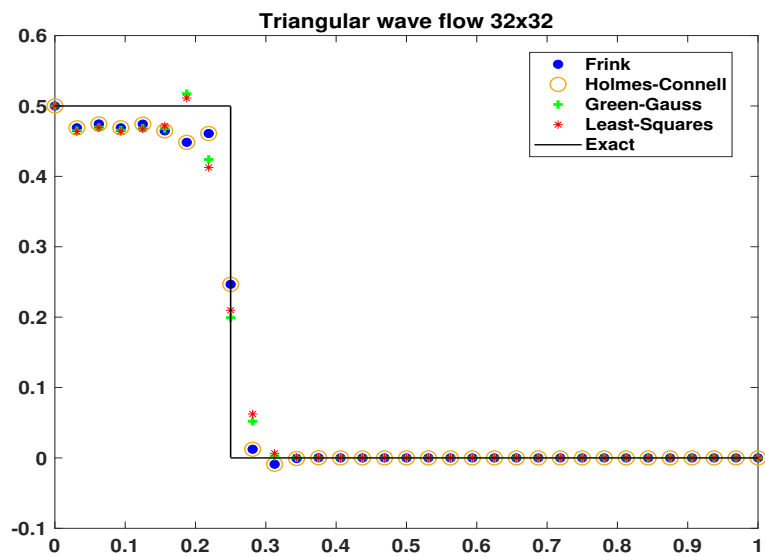


Figure 17: Comparison of the solutions of problem 4.3 on grid S2.

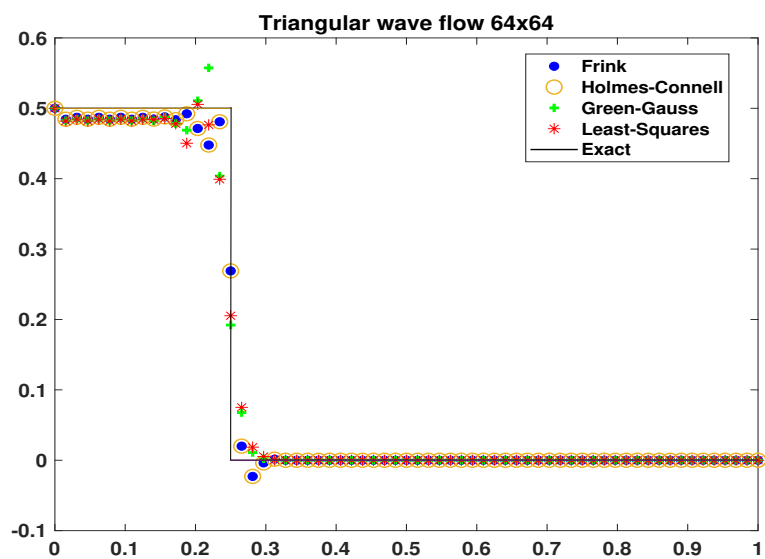


Figure 18: Comparison of the solutions of problem 4.3 on grid S3.

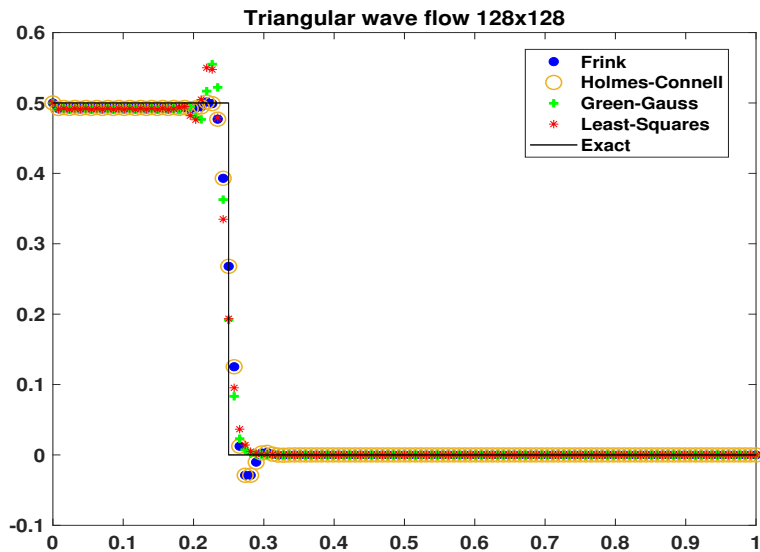


Figure 19: Comparison of the solutions of problem 4.3 on grid S4.

all examples, with the Frink and the Holmes-CConnell methods giving nearly identical solutions of lower accuracy. For all examples, the Green-Gauss method gave the least accurate solutions.

References

- [1] M. Aboubacar and M. F. Webster. Development of an optimal hybrid finite volume/element method for viscoelastic flows. *Int. J. Numer. Methods Fluids*, 41:1147, 2003.
- [2] J. P. Arachchige and G. J. Pettet. A finite volume method with linearisation in time for the solution of advection–reaction–diffusion systems. *Appl. Math. Comput.*, 231:445, 2014.
- [3] T. J. Barth. A 3-d upwind euler solver for on unstructured meshes. *AIAA Paper-91-1548*, 1991.
- [4] T. J. Barth and D. C. Jespersen. The design and application of upwind schemes on unstructured meshes. *AIAA Paper-89-0366*, 1989.
- [5] E. Bertolazzi and G. Manzini. A finite volume method for transport of contaminants in porous media. *Appl. Numer. Math.*, 49:291, 2004.
- [6] C. Chen, W. Liu, and C. Bi. A two-grid characteristic finite volume element method for semilinear advection-dominated diffusion equations. *Numer. Methods Partial Differ. Equ.*, 29:1543, 2013.
- [7] D. A. Di Pietro and A. Ern. *Mathematical Aspects of Discontinuous Galerkin Methods*, 2012.

- [8] J. Donea, B. Roig, and A. Huerta. High-order accurate time-stepping schemes for convection-diffusion problems. *Comput. Methods in Appl. Mech. Eng.*, 182:249, 2000.
- [9] R. Eymard, T. Gallouët, and R. Herbin. Finite volume methods. *Handbook of numerical analysis*, 7:713, 2000.
- [10] A. Filimon, M. Dumbser, and C. D. Munz. High-order finite volume schemes based on defect corrections. *Z. Angew. Math. Mech.*, 93:423, 2013.
- [11] N. T. Frink, P. Parikh, and S. Z. Pirzadeh. Fast upwind solver for the euler equations on three-dimensional unstructured meshes. *AIAA Paper-91-0102*, 1991.
- [12] C. Gallo and G. Manzini. Finite volume/mixed finite element analysis of pollutant transport and bioremediation in heterogeneous saturated aquifers. *Int. J. Numer. Methods Fluids*, 42:1, 2003.
- [13] F. Gao and Y. Yuan. The characteristic finite volume element method for the nonlinear convection-dominated diffusion problem. *Comput. Math. Appl.*, 56:71, 2008.
- [14] D. G. Holmes and S. D. Connell. Solution of the 2d navier-stokes equations on unstructured adaptive grids. *AIAA Paper-89-1932-CP*, 1989.
- [15] B. Lan, Z. Sheng, and G. Yuan. A new positive finite volume scheme for two-dimensional convection-diffusion equation. *Z. Angew. Math. Mech.*, 99:1, 2019.
- [16] Z. Lin and Q. Zhang. High-order finite-volume solutions of the steady-state advection-diffusion equation with nonlinear robin boundary conditions. *J. Comput. Phys.*, 345:358, 2017.
- [17] W. Liu, J. Huang, and X. Long. Coupled nonlinear advection-diffusion-reaction system for prevention of groundwater contamination by modified upwind finite volume element method. *Comput. Math. Appl.*, 69:477, 2015.
- [18] K. W. Morton and D. F. Mayers. *Numerical Solution of Partial Differential Equations*, 2003.
- [19] P. Nithiarasu, R. Codina, and O. C. Zienkiewicz. The characteristic-based split (cbs) scheme—a unified approach to fluid dynamics. *Int. J. Numer. Methods in Eng.*, 66(10):1514, 2006.
- [20] S. Phongthanapanich and P. Dechaumphai. A characteristic-based finite volume element method for convection-diffusion-reaction equation. *Trans. of the CSME*, 32:549, 2008.
- [21] S. Phongthanapanich and P. Dechaumphai. Combined finite volume and finite element method for convection-diffusion-reaction equation. *J. Mech. Sci. Technol.*, 23:790, 2009.
- [22] S. Phongthanapanich and P. Dechaumphai. Explicit characteristic finite volume method for convection-diffusion equation on rectangular grids. *J. Chin. Inst. Eng.*, 34:239, 2011.

- [23] S. Phongthanapanich and P. Dechaumphai. An explicit characteristic finite volume element method for non-divergence free convection–diffusion–reaction equation. *Int. J. Adv. Eng. Sci. Appl. Math.*, 4:179, 2012.
- [24] J. A. Pudykiewicz. Numerical solution of the reaction–advection–diffusion equation on the sphere. *J. Comput. Phys.*, 213:358, 2006.
- [25] B. M. Slepchenko, J. C. Schaff, and Y. S. Choi. Numerical approach to fast reactions in reaction-diffusion systems: application to buffered calcium waves in bistable models. *J. Comput. Phys.*, 162:186, 2000.
- [26] P. Tamamidis. A new upwind scheme on triangular meshes using the finite volume method. *Comput. Methods in Appl. Mech. Eng.*, 124(1-2):15–31, 1995.
- [27] A. Tambue. An exponential integrator for finite volume discretization of a reaction–advection–diffusion equation. *Comput. Math. Appl.*, 71:1875, 2016.
- [28] J. H. M. ten Thije Boonkkamp and M. J. H. Anthonissen. The finite volume-complete flux scheme for advection-diffusion-reaction equations. *J. Sci. Comput.*, 46:47, 2011.
- [29] P. Theeraek, S. Phongthanapanich, and P. Dechaumphai. Solving convection-diffusion-reaction equation by adaptive finite volume element method. *Math. Comput. Simulat.*, 82:220, 2011.
- [30] V. Venkatakrishnan. Convergence to steady state solutions of the euler equations on unstructured grids with limiters. *J. Comput. Phys.*, 118(1):120–130, 1995.
- [31] H. Wang and J. Liu. Development of cfl-free, explicit schemes for multidimensional advection-reaction equations. *SIAM J. Sci. Comput.*, 23:1418, 2001.
- [32] M. Xu. A modified finite volume method for convection-diffusion-reaction problems. *Int. J. Heat Mass Transf.*, 117:658, 2018.
- [33] C. Yang and L. M. Tine. A hybrid finite volume method for advection equations and its applications in population dynamics. *Numer. Methods Partial Differ. Equ.*, 33:1114, 2017.
- [34] Q. Zhang, H. Johansen, and P. Colella. A fourth-order accurate finite-volume method with structured adaptive mesh refinement for solving the advection-diffusion equation. *SIAM J. Sci. Comput.*, 34:B179, 2012.
- [35] O. C. Zienkiewicz and R. Codina. A general algorithm for compressible and incompressible flow—part i. the split, characteristic-based scheme. *Int. J. Numer. Methods Fluids*, 20(8-9):869, 1995.